ARMY RESEARCH LABORATORY

Multifunctional Structural-Energy Storage Nanocomposites for Ultra Lightweight Micro Autonomous Systems (First-year Report)

by Mark L. Bundy, Daniel P. Cole, Monica Rivera, and Shashi P. Karna

ARL-MR-0808 **February 2012**

NOTICES

Disclaimers

The findings in this report are not to be construed as an official Department of the Army position unless so designated by other authorized documents.

Citation of manufacturer's or trade names does not constitute an official endorsement or approval of the use thereof.

Destroy this report when it is no longer needed. Do not return it to the originator.

Army Research Laboratory
Aberdeen Proving Ground, MD 21005

ARL-MR-0808 **February 2012**

Multifunctional Structural-Energy Storage Nanocomposites for Ultra Lightweight Micro Autonomous Systems (First-year Report)

Mark L. Bundy
Vehicle Technology Directorate, ARL

Daniel P. Cole and Monica Rivera
Motile Robotics, Inc.

Shashi P. Karna
Weapons and Materials Research Directorate, ARL

REPORT DOCUMENTATION PAGE		Form Approved OMB No. 0704-0188

1. REPORT DATE *(DD-MM-YYYY)*	2. REPORT TYPE	3. DATES COVERED (From - To)
February 2012	DRI	FY2011

4. TITLE AND SUBTITLE	5a. CONTRACT NUMBER
Multifunctional Structural-Energy Storage Nanocomposites for Ultra Lightweight Micro Autonomous Systems (First-year Report)	NNL 09AA00A
	5b. GRANT NUMBER
	5c. PROGRAM ELEMENT NUMBER

6. AUTHOR(S)	5d. PROJECT NUMBER
Mark L. Bundy, Daniel P. Cole, Monica Rivera, and Shashi P. Karna	FY11-VTD-009
	5e. TASK NUMBER
	5f. WORK UNIT NUMBER

7. PERFORMING ORGANIZATION NAME(S) AND ADDRESS(ES)	8. PERFORMING ORGANIZATION REPORT NUMBER
U.S. Army Research Laboratory ATTN: RDRL-VTM Aberdeen Proving Ground, MD 21005-5069	ARL-MR-0808

9. SPONSORING/MONITORING AGENCY NAME(S) AND ADDRESS(ES)	10. SPONSOR/MONITOR'S ACRONYM(S)
	11. SPONSOR/MONITOR'S REPORT NUMBER(S)

12. DISTRIBUTION/AVAILABILITY STATEMENT

Approved for public release; distribution is unlimited.

13. SUPPLEMENTARY NOTES

*Motile Robotics, Inc., Joppa, MD, 21085

14. ABSTRACT

Micro vehicles (MVs) are projected to play an increasing role in both civilian and military applications. However, even with minimal payload, present day battery powered micro aerial vehicles (MAVs) have time-of-flights measured in minutes, woefully short for military applications. Since battery mass already accounts for a significant portion of the overall system mass, increasing battery size to boost MV endurance is not the solution. On the other hand, if the energy storage device can be efficiently integrated into the vehicle structure, serving multiple functions, it could increase endurance by reducing parasitic mass. Unlike larger vehicles, MVs are generally made from lightweight, flexible materials; hence, an integrated power source should have similar characteristics. The research reported herein focuses on preliminary results and progress in a Director's Research Initiative project focused on the design and fabrication of lightweight, flexible power sources, ultimately intended for integration into the structural features of MVs.

15. SUBJECT TERMS

Carbon nanotubes, CNTs, supercapacitor, multifunctional, energy, structural-Energy

16. SECURITY CLASSIFICATION OF:			17. LIMITATION OF ABSTRACT	18. NUMBER OF PAGES	19a. NAME OF RESPONSIBLE PERSON
a. REPORT	b. ABSTRACT	c. THIS PAGE			Mark Bundy
Unclassified	Unclassified	Unclassified	UU	40	19b. TELEPHONE NUMBER (*Include area code*) (410) 278-4318

Standard Form 298 (Rev. 8/98)
Prescribed by ANSI Std. Z3

Contents

List of Figures

List of Tables

Acknowledgments

We would like to thank Arava L. M. Reddy, Myung G. Hahm, Robert Vajtai, and Pulickel M. Ajayan of Rice University for providing us with the vertically aligned carbon nanotube (CNT) forests used in this project and for helpful discussions on CNT-based energy storage devices. We would also like to thank Matthew H. Ervin of the Sensors and Electronic Devices Directorate, U.S. Army Research Laboratory (ARL), for helpful feedback on the report and the research.

INTENTIONALLY LEFT BLANK.

1. Objective

The proposed research plan seeks to combine the emerging area of multifunctional lightweight energy storing materials with the existing large-scale structural battery/capacitor technology to accomplish the following:

1. Develop ultra-light, structurally robust, nanocomposite energy storage materials.
2. Characterize their structure-electrical/mechanical relationships, as well as the electromechanical coupling effects.
3. Characterize environmental effects on electro-mechanical performance.

2. Approach

2.1 Introduction

A reoccurring issue for lightweight (mass < 100 g), palm-sized, micro vehicle (MV) platforms, and in particular micro aerial vehicle (MAV) platforms, is the lack of sufficient onboard power. Stringent size and weight constraints and demanding voltage and power requirements significantly limit the number and type of energy storage devices that can be housed in MVs. While most commercial and developmental MVs currently use commercial-off-the-shelf (COTS) lithium polymer batteries for their energy storage needs, the capacity of these batteries can limit mission durations to the order of minutes and the weight of these batteries can account for up to 60% of the overall system mass (*1*). One method to increase the vehicle endurance without adding mass to the system or sacrificing payload capabilities is to incorporate multiple functions into a single material or structure. For example, the body or chassis of a MV could be replaced with a multifunctional material that would serve as both the vehicle structure and the energy storage device.

One of the primary structural characteristics of biomimetic MVs is their inherent flexibility. As seen in figure 1, the flexibility of the Dynamic Autonomous Sprawled Hexapod (DASH) 16-g hexapedal robot allows the small ground-based robotic platform to withstand falls from large heights (28 m or 280 body lengths) by absorbing energy on ground impact (*2*). Another example is the “flexible, twisty, wing structure” of the Defense Advanced Research Projects Agency (DARPA) Bug, which enables the vehicle to generate lift on both the upstroke and downstroke by reversing the twist and camber (*3*). The structural supports of biomimetic MVs are typically flexible, polymer-based materials, such as common plastics or cellulose. Hence, a suitable structure-serving energy source for MVs should also be flexible.

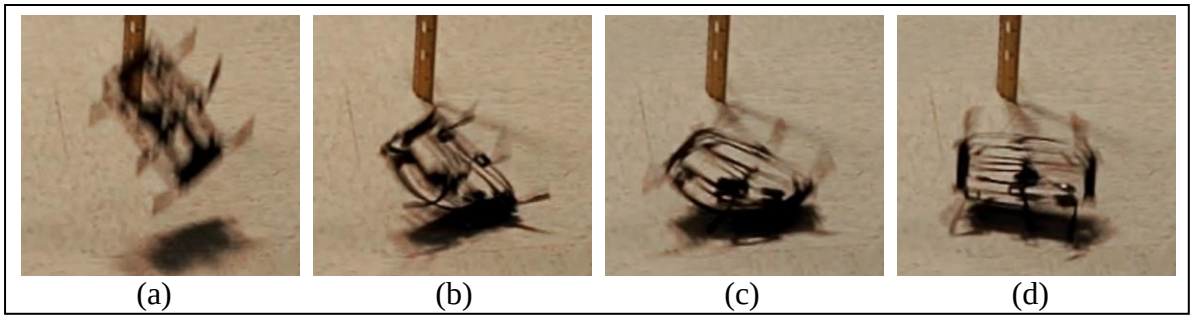

Figure 1. Images of DASH impacting the ground at a velocity of approximately 6.5 m/s. (b) and (c) show the great contortion that the body undergoes during impact. By (d), the body has almost fully recovered to its original shape (a). Image reproduced from reference 2.

While the concept of a structural-energy storage device is not new (*4–9*), most structural-energy storage research has focused on high stiffness materials for large (meter-scale) devices. For instance, early structural-energy storage work by Luo et al. (*4*) focused on structural capacitors based on carbon fiber (tensile modulus = 221 GPa, tensile strength = 3.1 GPa), paper, and epoxy (flexural modulus = 3.7 GPa, flexural strength = 138 MPa). Within the U.S. Army Research Laboratory (ARL), lightweight, structural, energy-storing materials—derived from polymers, resins, and carbon-fiber electrodes—have been studied for potential applications in manned vehicles (*10–18*) and man-portable unmanned vehicles (*19*). In related research, ARL has also investigated using carbon nanotube (CNT)-based electrodes for general purpose (*20, 21*) and flexible (*22*) energy storage applications. Likewise, the research reported in this Director's Research Initiative (DRI) report relies on CNT-based electrodes for flexible energy storage devices, with the particular application of providing both structural support and power to MVs.

2.2 Carbon Nanomaterial-based Energy Storage Research

Since the discovery of CNTs, and more recently graphene, there has been a significant amount of research on using the high surface area and conductivity of these materials for battery and supercapacitor electrodes (*20–31*). Because CNT-based electrodes do not rely on thin, continuous films that are vulnerable to cracking, they retain conductivity even at large strains (*32, 33*). As a result, these nanomaterial-based energy storage devices are ideal candidates for flexible MV applications.

Although carbon nanomaterial-based energy storage device research is an extremely active area of study, little is known about the complex interaction between the electrical and mechanical properties of these devices. While some researchers have begun to examine the electrical properties of CNT-based energy storage devices before, during, and after steady-state mechanical loading (*30, 34*), little information is known about the electrical properties during time-variant mechanical loading. Since composites have also been explored as strain sensors (*35–39*), the electromechanical coupling in carbon nanomaterial-based energy storage devices must be investigated if these devices are to be successfully incorporated into MV platforms. While in-situ mechanical and electrical characterization is a major part of the proposed DRI

research, the year 1 studies focused on non-coupled electrical and mechanical characterization techniques.

2.3 Materials and Methods

The electrodes of supercapacitors and batteries are similar in that the electrical conductivity and the available surface area of the electrode material strongly affect the overall device performance, with larger values typically leading to better electrical performance. Carbon nanomaterial-based supercapacitors, however, are easier to manufacture and test than carbon nanomaterial-based batteries as the mirrored device architecture of a supercapacitor facilitates device assembly and the reversible charge storage mechanism of electrical double layer capacitors (EDLCs) results in enhanced device stability. For these reasons, year 1 studies focused on the development of carbon nanomaterial-based supercapacitors. CNTs were selected as the carbon nanomaterial of choice in year 1 of the project as they are cheaper and more readily available than graphene sheets or flakes.

CNT-based electrodes can be fabricated in a random or aligned fashion. Randomly oriented CNT-based electrodes (ROEs) typically consist of CNT inks or solutions that are directly deposited onto a solid matrix or current collector (*20–22, 29*) or randomly dispersed within a polymer matrix (*30*). Vertically aligned CNT-based electrodes (VAEs), on the other hand, typically consist of vertically aligned CNT forests that are infiltrated with a matrix material (*24*) or inserted into a polymer electrolyte membrane (*40*). Figure 2 contains a conceptual drawing of multifunctional structural-energy storage device based on vertically aligned CNT-based electrodes. As both CNT-based electrode morphologies have exhibited promising electrical behavior, we chose to examine both morphologies in year 1 of the DRI project. The following subsections describe the fabrication, modification, and characterization of the supercapacitors constructed from these CNT-based electrode materials.

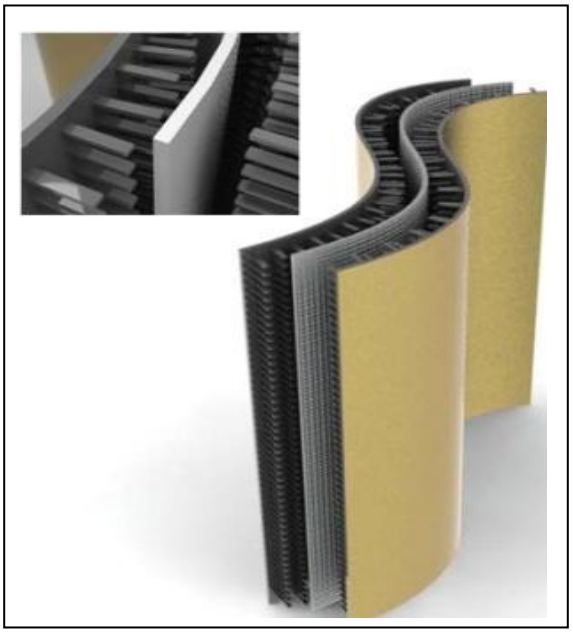

Figure 2. Conceptual drawing of a multifunctional structural-energy storage nanocomposite based on vertically aligned CNT-based electrodes. The inset shows a close up of the electrode/separator/electrode interface.

2.3.1 Randomly Oriented CNT-based Electrodes

The electrical properties of two different randomly oriented CNT electrode compositions were studied in year 1 of the DRI project. Randomly oriented electrode composition #1 (ROE_1) consisted of a conductive CNT composite (Cheap Tubes, Inc., outer diameter = 60–80 nm) and a polyvinylidene fluoride (PVDF) binder material and random electrode composition #2 (ROE_2) consisted of multi-walled nanotubes (MWNTs) (Cheap Tubes, Inc., outer diameter <8 nm), carbon black, and PVDF. Each electrode composition was dispersed in dimethylformamide (DMF) and deposited onto one side of a stainless steel current collector (described in section 2.3.3). After drying, the current collector/electrode systems were weighed and the effective electrode mass was calculated. Figure 3a contains a picture of a random CNT electrode deposited on a stainless steel current collector.

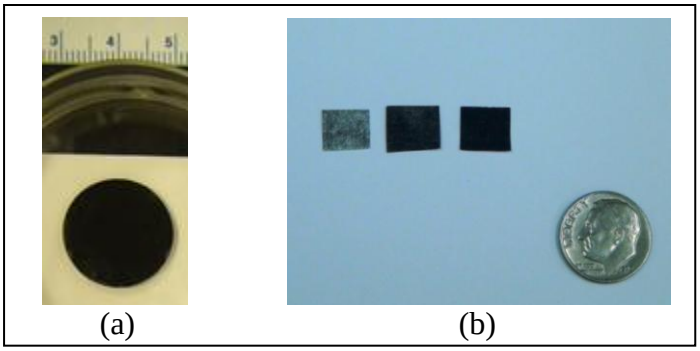

Figure 3. CNT-based supercapacitor electrodes. (a) ROE on stainless steel current collector. (b) ROEs on commercial paper substrates processed via doctor blade technique.

In order to determine the effect of separator porosity and thickness on device performance, randomly oriented CNT electrodes (ROE_1 and ROE_2) were processed in a batch-wise fashion. As four separator materials were used in our initial studies, each random CNT electrode batch consisted of eight electrodes. The separator materials are discussed in greater detail in section 2.3.4.

The mechanical properties of randomly oriented CNT-paper electrodes were also studied in year 1 of the DRI project. Flexible CNT-ink-based electrodes were processed through a technique first reported by Hu et al. (*29*) and also used by Anton et al. (*22*). Inks were processed by dispersing MWNTs (Cheap Tubes, Inc., outer diameter <8 nm) in various solvents, including deionized water (DI-H_2O) and DMF. For the DI-H_2O based inks, a surfactant, sodium dodecylbenzenesulfonic acid (SDBS), was used to help disperse the CNTs. The CNT-ink solution was mixed via magnetic stirring for 30 min and then sonicated using a Sonics VibraCell probe sonicator at 200 W for 30 min. Immediately following the sonication, the solution was mixed for an additional 30 min via magnetic stirring. The CNT-ink solution was cast onto commercial printing paper using both the Meyer rod technique (*29*) and doctor blade technique (*41*). Figure 3b shows an image of three randomly oriented CNT ink-based electrodes processed via the doctor blade technique. From left to right, the image shows electrodes with one, two, and three CNT ink applications. Multiple depositions were required to fully coat the paper-based electrodes. This could potentially be due to CNT agglomerates that were still present in the ink after the stirring and sonication steps.

2.3.2 Vertically Aligned CNT-based Electrodes

Vertically aligned CNT forests were grown via a water-assisted chemical vapor deposition (CVD) method by collaborators at Rice University (*42*). A catalyst layer consisting of aluminum (~10 nm) and iron (~1.5 nm) was first sputter deposited onto silicon wafers. For the CVD process, the carbon source used was ethylene gas, while an argon/hydrogen mixture run through a water bubbler was used as the carrier gas. The aligned CNTs were grown in a tube furnace held at 775 °C. Figure 4 shows scanning electron microscope (SEM) and transmission electron

microscope (TEM) images of the vertically aligned CNT forests. The TEM images were used to show that the CNTs contained anywhere from 5–10 walls and had an outer diameter in the range of 5–15 nm.

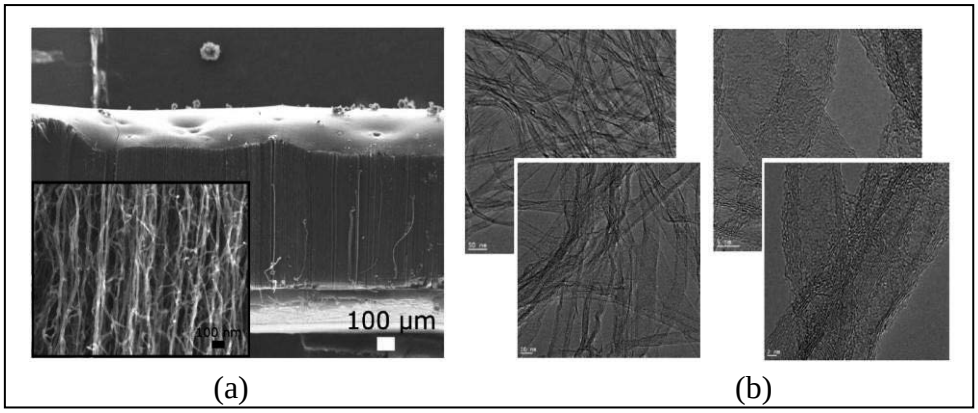

Figure 4. (a) SEM and (b) TEM images of vertically aligned CNTs grown via CVD (images provided by Rice University.)

Flexible, aligned CNT composite electrodes were fabricated by infiltrating the forests with a mixture of 80–90 wt.% of polydimethylsiloxane (PDMS) and 10–20 wt.% of PVDF. PDMS was used to increase the flexibility of the composite, while the PVDF was chosen to bind the active electrode material together. The liquid polymer solution was magnetically stirred for 30 min, followed by probe sonication at 200 W for 15 min, and then magnetically stirred for another 30 min. The solution was then put under a low vacuum for 30 min to remove air bubbles from the solution. The de-gassed liquid polymer was then poured on top of the aligned CNTs and allowed to infiltrate the forest. After allowing the composite to cure overnight, the sample was lifted off from the substrate using a razor blade. Figure 5a displays the flexibility of the aligned CNT-PDMS/PVDF composite electrode. The mass of CNTs (M_{CNT}) in each composite electrode was approximated by weighing: (1) the CNT forest (A) and silicon wafer (B) prior to polymer infiltration (M_1 = A+B), (2) the CNT forest-polymer (C) composite and silicon wafer after complete curing, (M_2 = A+B+C) (3) the silicon wafer (after removing composite) (M_3 = B), and then subtracting the mass in step 3 from the mass in step 1 ($M_{CNT} = M_1 - M_3 =$ A+B-B = A). This information was used to approximate the CNT weight fraction in the composite electrode (CNT wt.% = $(M_1-M_3)/(M_2-M_3)$).

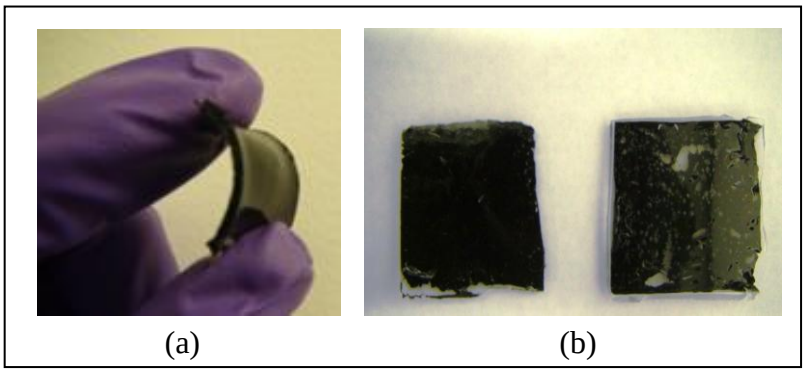

Figure 5. (a) Photograph displaying the flexibility of the aligned CNT-PDMS/PVDF composite electrode. (b) Photograph shows aligned CNT-PDMS/PVDF composite electrode with vacuum treatment (left) and without vacuum treatment (right).

We note that several combinations of polymers/solvents were attempted for the forest infiltration process; however, the solutions containing solvents tended to cause the forests to collapse. The collapsing effect was thought to be a result of relatively high capillary forces acting on the loosely rooted CNTs in the presence of a solvent. The selection of the solvent-free PDMS/PVDF solution allowed CNT architecture to remain mostly intact, although as figure 5b shows, the forest still collapsed in some areas. This was thought to be a result of air bubbles that formed in the liquid polymer during the magnetic stirring and probe sonication steps. The vacuum treatment step prior to infiltration was effective in removing the air bubbles and preserving the alignment of the forest. SEM of the composite cross section is still required in order to verify the alignment. The ability to preserve the CNT alignment during infiltration was a key step in the processing of the electrodes, as even a partially collapsed CNT forest was expected to result in a greatly reduced capacitance due to the large reduction in electrode surface area.

2.3.3 Current Collectors

Although copper and silver are predominantly used as current collectors in the commercial battery industry (*43*) and aluminum and nickel current collectors have been used in previous ARL studies (*20–22*), stainless steel 304 sheets were used as the current collectors of the randomly oriented CNT-based electrode (ROE_1 and ROE_2) devices in an effort to match the electrical resistivity of the supercapacitor current collector to the Swagelok electrical test cell. While this material substitution precludes a direct comparison with COTS supercapacitor devices, it will allow us to directly compare the performance of our prototypes and gauge whether or not the design is worth pursuing.

Electron Microscopy Sciences silver adhesive 503 (62 wt.% solid) was used as the current collectors of the vertically aligned CNT-based (VAE_1) supercapacitors. The silver paint was applied to the electrode surface and allowed to dry overnight.

2.3.4 Separator Materials

Whatman qualitative cellulose filter papers were used as the separator material for the CNT-based supercapacitors. In order to determine the effect of porosity and thickness on supercapacitor performance, four different grades (1, 2, 3, and 5) of cellulose filter paper were examined in year 1 of the project. Manufacturer supplied material properties of the cellulose filters can be found in table 1. Filter paper separators were cut to size and weighed before being inserted into the Swagelok electrical test cell.

Table 1. Manufacturer supplied cellulose filter paper properties.

Sample ID	Sample Grade	Particle Retention (Liquid) (µm)	Typical Thickness (µm)	Dry Tensile Strength (MD) (N/15 mm)
G_1	1	11	180	39.1
G_2	2	8	190	44.6
G_3	3	6	390	72
G_5	5	2.5	200	55.6

Note: MD = machine direction and Particle Retention (Liquid) = particle size at which a retention level of 98% of the total number of particles initially challenging the filter is obtained (*48*).

2.3.5 Electrolytes

6M potassium hydroxide (KOH) was used as the aqueous electrolyte in the randomly oriented CNT-based supercapacitors (ROE_1 and ROE_2). A 1M solution of lithium hexafluorophosphate ($LiPF_6$) in 1:1 volume/volume mixture of ethylene carbonate (EC) and dimethyl carbonate (DMC) was used as the electrolyte for the vertically aligned CNT-based supercapacitors (VAE_1). The $LiPF_6$-based electrolyte was prepared and handled in an Omni-lab glove box system (Vacuum Atmospheres Company) filled with argon gas. The amount of electrolyte used in individual tests was based on the amount of solution necessary to fully wet the separator (determined visually).

2.3.6 Supercapacitor Assembly

All supercapacitors were assembled in a modified two electrode Swagelok cell (figure 6a and b). The modified Swagelok electrical test cell consists of a stainless steel Swagelok ultra-torr vacuum fitting (SS-16-UT-6BT), a solid stainless steel cylinder, and a spring-loaded plate-cylinder assembly. KOH-based supercapacitors were assembled in an ambient environment and $LiPF_6$-based supercapacitors were assembled in the inert environment of the glove box. The Swagelok ultra-torr vacuum fitting is ideal for basic supercapacitor and battery research as it allows for quick and easy single device assembly and prevents electrolyte evaporation and contamination during prolonged electrical characterization. The spring mechanism in the test cell applies a constant, even pressure to the current collectors throughout the test process, thereby ensuring that adequate contact is made between the supercapacitor sub-components. In

order to ensure that current only travels through the device under test (DUT) and not through the Swagelok fitting, the fitting is electrically isolated from the stainless steel cylinder, DUT, and spring-loaded plate-cylinder assembly via 3M transparency film (PP22500).

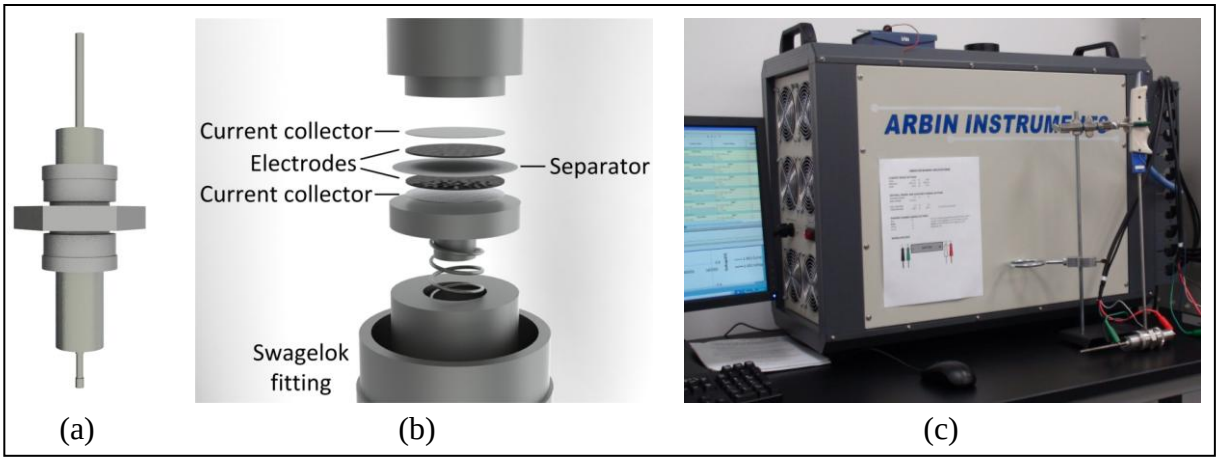

Figure 6. Electrical characterization equipment: (a) assembled Swagelok electrical test cell, (b) expanded view of the Swagelok electrical test cell with supercapacitor components, and (c) Arbin Instruments Supercapacitor Test System with the assembled Swagelok electrical test cell.

Supercapacitors are assembled in a bottom-up process by first placing the current collector/electrode into the test cell, with the current collector facing the solid stainless steel cylinder. Once the bottom current collector/electrode is in place, the separator material is carefully placed on top of the electrode inside the test cell. After wetting the separator with electrolyte, the top current collector/electrode is placed into the test cell with the electrode facing the wet separator. Once the top current collector/electrode is in place, the spring-loaded plate-cylinder assembly is inserted into the open end of the Swagelok vacuum fitting and placed on the exposed current collector. The Swagelok electrical test cell is then sealed and prepped for electrical characterization.

2.4 Electrical Characterization

To verify the electrical properties of the current collectors, the resistivity of a subset of the stainless steel current collectors was measured on a Cascade Microtech semiautomatic probe station with a Keithley 4200 Semiconductor Characterization System using the van der Pauw method. Because resistivity is dependent on the thickness of the sample, a number of steps were taken to minimize errors due to thickness. Specifically, the sample thickness used in the resistivity calculations was the average thickness of 10 measurements made on the same sample and the average resistivity value was calculated from 50 resistivity measurements made at five different *xy* locations on the sample.

Cyclic voltammetry (CV), self-discharge, and galvanostatic charge-discharge test schedules were developed in the MITS Pro Testing Software (Arbin Instruments) and implemented on an Arbin Instruments Supercapacitor Testing System (figure 6c). During electrical characterization tests,

current, voltage, cell temperature, and ambient temperature readings were recorded at a frequency no less than 0.2 Hz, depending on the test step and/or the change in current or voltage. Cell temperature was measured by placing a flexible tip surface probe (type T) thermocouple on the exterior of the Swagelok electrical test cell.

2.5 Mechanical Characterization

The mechanical properties of the randomly oriented CNT-ink electrodes and the vertically aligned CNT-based electrodes were characterized via an Instron 5965 Materials Testing System with a 500 N load cell (figure 7). Pneumatic grips were used in order to apply a constant pressure to the materials and prevent slipping during loading. For the paper-based electrodes, groups of five specimens were tested at various strain rates, and the average tensile strength and elastic modulus were determined via the Technical Association of the Pulp and Paper Industry (TAPPI) T494om-96 standard for mechanical testing (*44*). All tests were run at room temperature. The effects of temperature and humidity on mechanical performance will be explored in year 2 of the project.

(a) (b)

Figure 7. (a) Instron Materials Characterization System with (b) pneumatic grips.

3. Results

3.1 Mechanical Results

3.1.1 Randomly Oriented CNT-paper Electrodes

Initial mechanical tests were performed on commercial printing paper to determine the baseline substrate properties prior to CNT ink deposition. Commercial paper is typically manufactured from a slurry composed of water and 0.5–1.0% pulp fiber. The free standing paper is formed on a moving wire mesh that drains the water. The fibers tend to align with the direction of motion of the wire mesh, known as the machine direction (MD); the direction orthogonal to the MD is

referred to as the cross-machine direction (CD) (*44*). Figure 8 shows the orthotropic properties of the paper substrates used in this study. The tensile strength and elastic modulus of the paper loaded in the MD was approximately 250% higher than the paper loaded in the CD. The results also indicate that the mechanical behavior of the paper substrates is dependent on the strain rate. As the strain rate increased, the tensile strength and elastic modulus increased by approximately 10% and 15%, respectively.

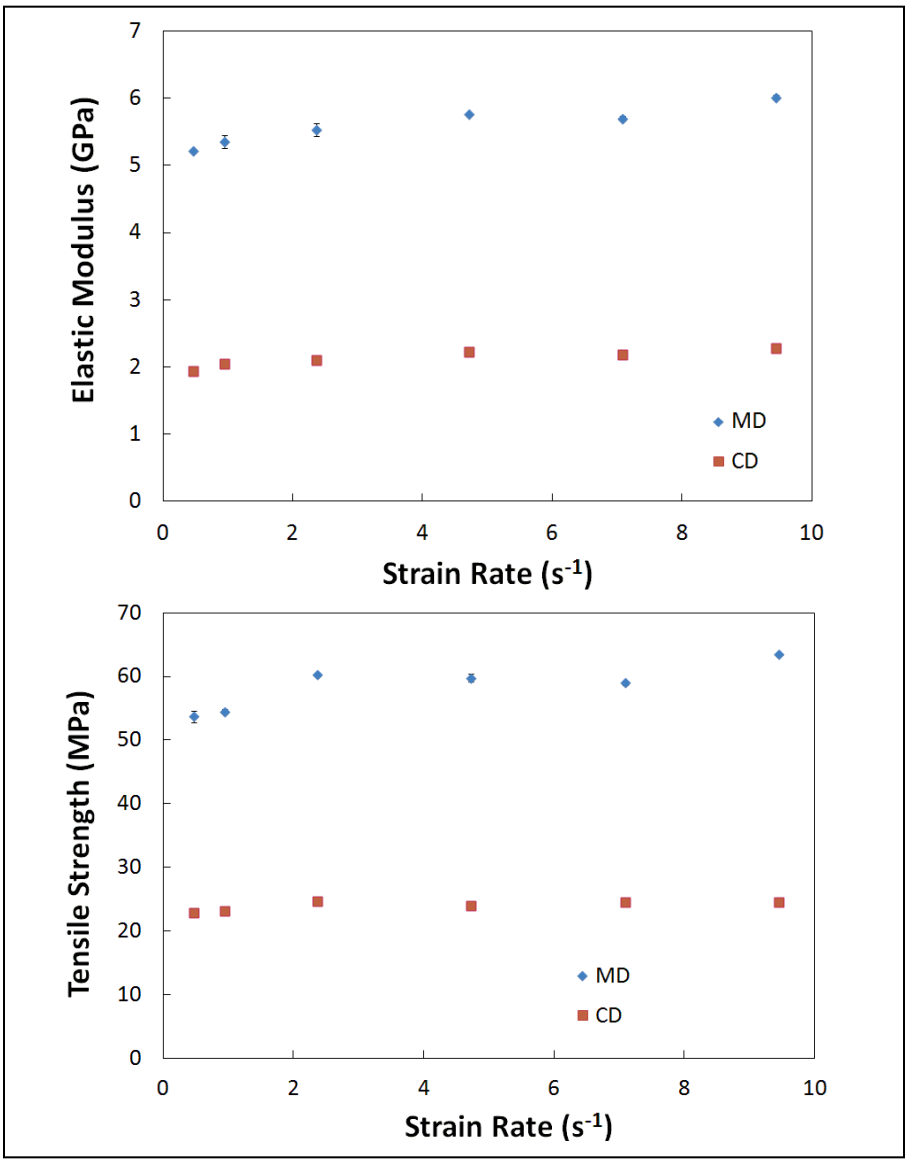

Figure 8. Elastic modulus and tensile strength of commercial paper substrates as a function of strain rate. Error bars are located within the data points unless otherwise noted.

Tests on the CNT-coated paper samples (processed through the doctor blade technique) were performed in the MD in order to determine the maximum mechanical properties. The specimens were loaded at both 1 and 5 mm/min. Figure 9 shows the average tensile strength and elastic modulus of the CNT-coated paper electrodes. A control sample coated with pure DMF (0 layer of CNT ink) demonstrates the effects of the solvent on the mechanical properties of the paper. The tensile strength is largely unaffected; however, the elastic modulus of the sample decreases by approximately 50% as a result of the DMF treatment. Tests on the CNT-coated specimens also indicate that the CNT deposition process degrades the mechanical properties of the paper. The application of a single layer of the CNT ink caused the average elastic modulus and tensile strength of the coated paper to decrease by approximately 15%, with respect to the pure DMF-coated paper. This could potentially be due to additional damage caused to the paper substrate from the more viscous CNT-DMF solution, which was more difficult to spread across the paper substrate. Multiple applications of the ink were required to fully coat the paper substrates. A second application of CNT ink caused the average mechanical properties of the composite to degrade further. The application of a third layer did not cause a further decrease in the mechanical performance.

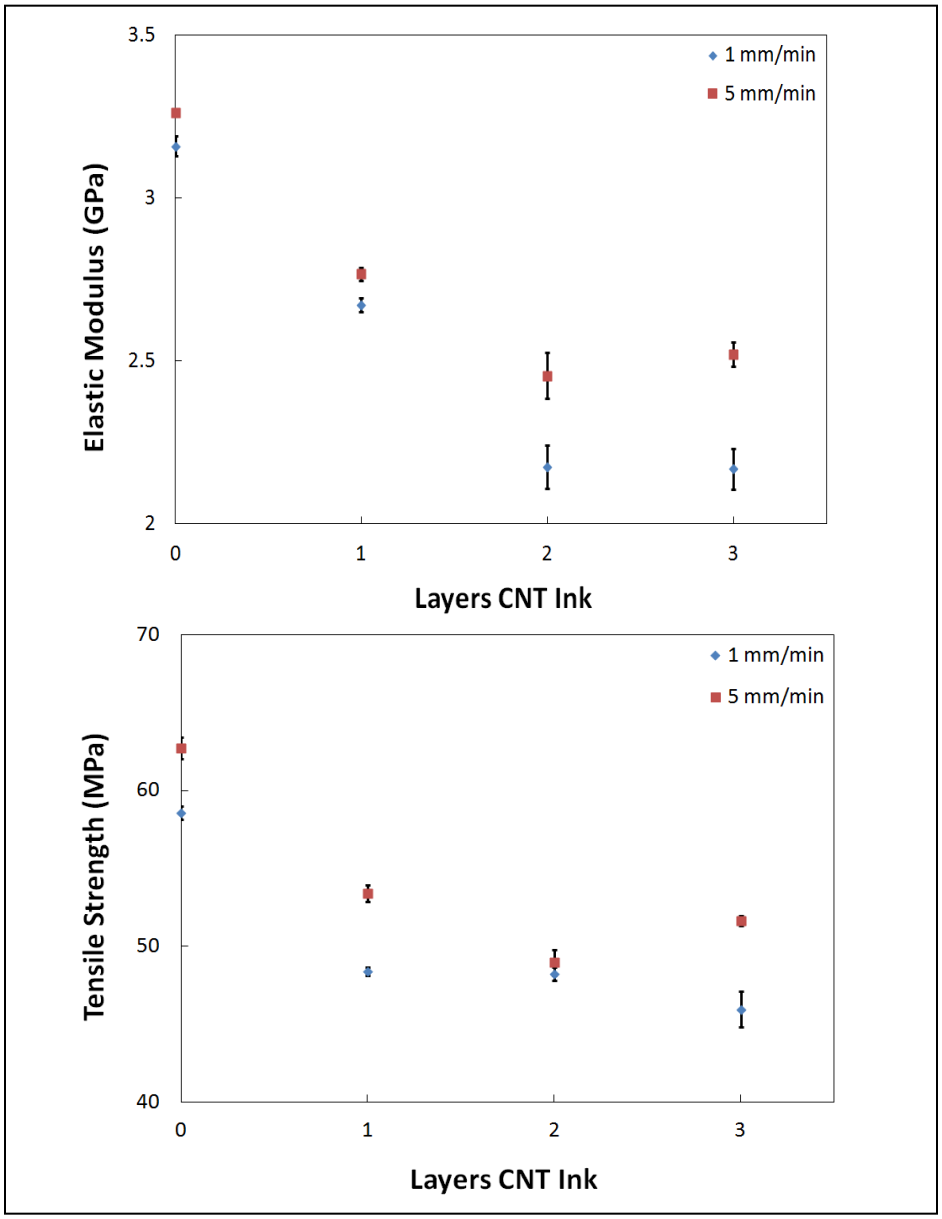

Figure 9. Elastic modulus and tensile strength of CNT-coated paper electrodes obtained through bulk tensile tests. Note that all specimens were tested in the MD. Error bars are located within data points unless otherwise noted.

3.1.2 Vertically Aligned CNT/Polymer Composite Electrodes

Uniaxial tensile tests were also performed on the vertically aligned CNT composite electrodes. Figure 10b compares the mechanical behavior of a neat PDMS (85 wt.%)–PVDF (15 wt.%) matrix and the same matrix loaded with 8 wt.% aligned CNTs. The specimens were loaded at a rate of 5 mm/min. The initial nonlinear portion of the loading curve corresponding to the specimen flattening was ignored; the initial linear behavior was used to calculate the elastic modulus.

The average elastic modulus of the composite electrode was approximately 2.5 times higher than the neat matrix. While the 250% increase in elastic modulus (E) is notable, the configuration of the composite electrode is not currently designed to maximize the mechanical properties. As the schematic in figure 10a shows, the CNTs are aligned transverse to the direction of loading. As a result, the configuration does not take full advantage of the stiffness of the CNTs, which is typically realized through aligning the filler with the direction of mechanical loading (*45*, *46*).

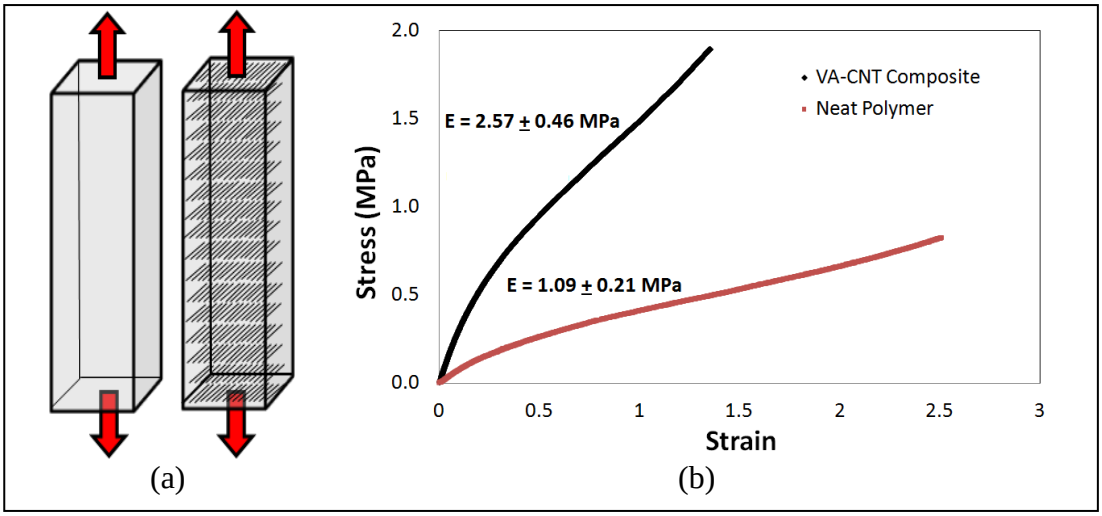

Figure 10. (a) Schematic shows the direction of mechanical loading with respect to the aligned CNTs and (b) stress-strain curve for a neat polymer matrix and an aligned CNT composite electrode.

3.2 Electrical Results

In an effort to characterize the electrical properties of the randomly oriented and vertically aligned CNT-based supercapacitors, a number of electrical characterization tests were conducted. The following sections outline the results of the galvanostatic charge-discharge, self-discharge, and CV tests.

3.2.1 Galvanostatic Charge-discharge Tests

In an effort to characterize the performance of the CNT-based supercapacitors, a number of constant current (or galvanostatic) charge-discharge measurements were made. Figure 11 contains the charge-discharge behavior of a randomly oriented and vertically aligned CNT-based supercapacitor. The charge-discharge curves of the randomly oriented CNT-based supercapacitors are similar to those reported in the literature (*24*, *29*, *34*).

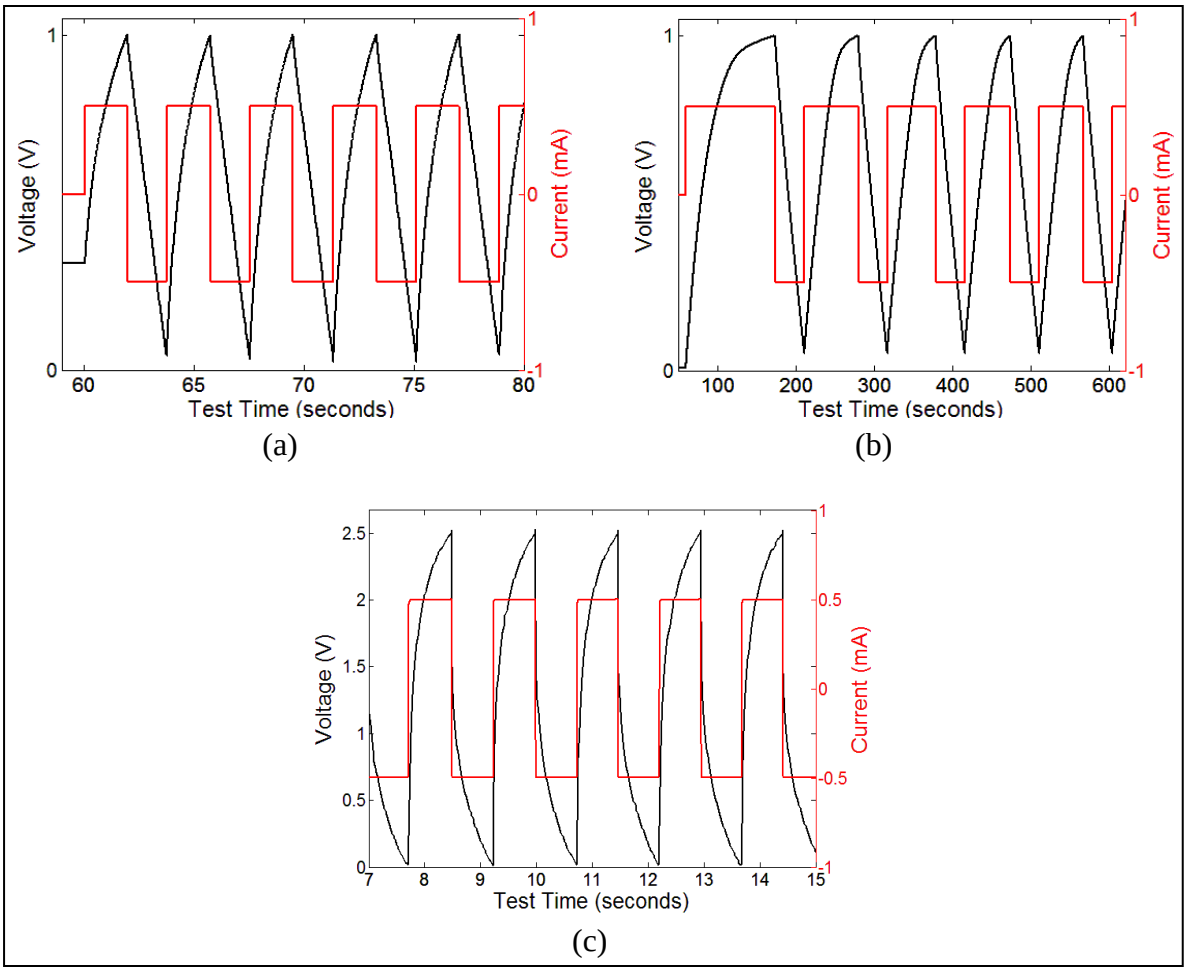

Figure 11. Galvanostatic charge-discharge curves (current = ±0.5 mA). Red is the applied current; black is the measured voltage. (a) ROE_1/G_2 supercapacitor, (b) ROE_2/G_2 supercapacitor, and (c) VAE_1/G_2 supercapacitor.

Table 2 contains the average charge times, discharge times, and specific capacitance with respect to full electrode mass (i.e., total mass of CNTs, carbon black, and PVDF in the two-electrode supercapacitor device) for the randomly oriented CNT-based supercapacitors. Because the supercapacitor behavior is cycle dependent, data from cycles >3 was averaged and reported (unless otherwise noted). As table 2 and figure 12 illustrates, the charge/discharge rate is dependent on the applied current, the separator material, and the electrode composition. ROE_1 supercapacitors exhibited significantly faster (6–27 times) charge and discharge times than ROE_2 supercapacitors. Of those randomly oriented CNT-based supercapacitors tested during the initial study, ROE_2/G_1 had the highest specific capacitance (5.8 F/g). While additional studies are currently underway, the diameter of the CNTs in ROE_1 and ROE_2 are believed to play a significant role in the specific capacitance of the device, with larger diameter CNTs having more "dead weight" than smaller diameter, fewer walled CNTs. Electrode composition and dispersion and deposition techniques are also being investigated as potential sources for specific

capacitance variations. The vertically aligned CNT composite electrodes displayed a much lower specific capacitance (~15 mF/g). This could potentially be the result of the poor ionic conductivity of the polymer matrix, which has not yet been optimized.

Table 2. Galvanostatic charge-discharge data.

$I_{c/d}$ (mA)	Sample ID	T_{charge} (s)	$T_{discharge}$ (s)	C_{sp} (F/g)	Sample ID	T_{charge} (s)	$T_{discharge}$ (s)	C_{sp} (F/g)
0.1	ROE_1/G_1	26 ± 1	17.26 ± 0.02	0.8	ROE_2/G_1	311 ± 16	152.4 ± 0.4	5.8
0.5	ROE_1/G_1	3.43 ± 0.07	2.98 ± 0.01	0.8	ROE_2/G_1	48 ± 5	28.5 ± 0.1	5.7
1.0	ROE_1/G_1	1.42 ± 0.03	1.29 ± 0.01	0.6	ROE_2/G_1	16.7 ± 0.4	14.86 ± 0.05	5.8
0.1	ROE_1/G_2	16.9 ± 0.5	12.1 ± 0.2	0.4	ROE_2/G_2[a]	1567 ± 587	192 ± 1	4.4
0.5	ROE_1/G_2	1.95 ± 0.02	1.81 ± 0.01	0.3	ROE_2/G_2	55 ± 3	36.67 ± 0.05	4.4
1.0	ROE_1/G_2	0.82 ± 0.03	0.74 ± 0.01	0.2	ROE_2/G_2	21.9 ± 0.2	18.69 ± 0.04	4.5
0.1	ROE_1/G_3[a]	2570	49	X	ROE_2/G_3[a]	632 ± 170	112.1 ± 0.8	4.3
0.5	ROE_1/G_3	4.19 ± 0.02	3.83 ± 0.02	0.9	ROE_2/G_3	24.7 ± 0.4	21.01 ± 0.03	4.2
1.0	ROE_1/G_3	1.79 ± 0.03	1.50 ± 0.01	0.7	ROE_2/G_3	12.5 ± 0.1	10.36 ± 0.01	4.2
0.1	ROE_1/G_5	20 ± 2	11.96 ± 0.03	0.5	ROE_2/G_5	282 ± 9	148.5 ± 0.3	4.9
0.5	ROE_1/G_5	2.09 ± 0.04	1.82 ± 0.01	0.4	ROE_2/G_5	35.0 ± 0.6	29.50 ± 0.02	5.1
1.0	ROE_1/G_5	0.91 ± 0.02	0.79 ± 0.01	0.4	ROE_2/G_5	15.5 ± 0.1	14.45 ± 0.03	5.0

[a]Did not reach 1 V during all cycles. Only those cycles that did reach 1 V were averaged.

Note: $I_{c/d}$ – charge/discharge current, T_{charge} – charge time, $T_{discharge}$ – discharge time, C_{sp} – specific capacity (calculated with respect to full electrode mass)

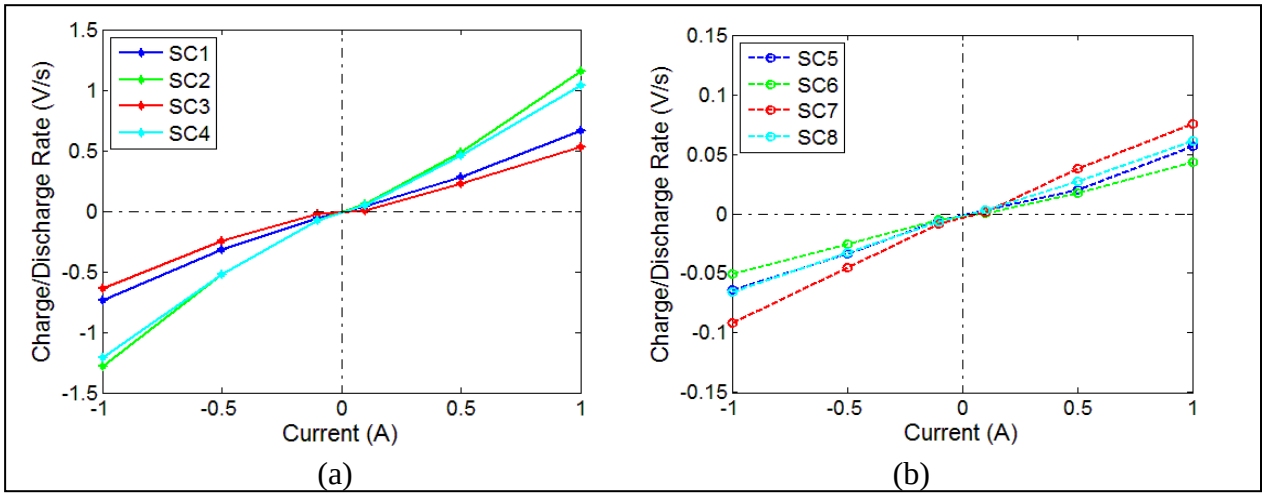

Figure 12. Charge/discharge rates with respect to applied current: (a) ROE_1 supercapacitor. (b) ROE_2 supercapacitor. Blue is G_1, green is G_2, red is G_3, and cyan is G_5.

Note: SC – supercapacitor.

3.2.2 Self-discharge Tests

The self-discharge behavior of a supercapacitor is a key indicator of device performance as the spontaneous loss of voltage causes the capacitor to approach a condition where energy is

required to reset the device to the charged, functional state. As a result, capacitors with lower self-discharge (or leakage) are typically more desirable, from an electrical standpoint, than those with higher self-discharge.

The self-discharge behavior of the randomly oriented CNT supercapacitors was measured using two different methodologies. In the first method, the supercapacitor was charged to the desired potential (1 V) and held at that potential for a given period of time (30 or 60 min). The residual current flow needed to keep the supercapacitor fully charged was averaged over the course of the constant voltage hold time (T_h) and was recorded as the supercapacitor float current (I_{float}). The second method is similar to the first with the exception that instead of measuring the float current during the hold period, the voltage of the device is measured after the charging current is removed from the device. For this experiment, the voltage was recorded until the potential reached the lower cutoff threshold (50 mV) or until the voltage decay time (T_{decay}) exceeded 2 h, whatever occurred first. Because the supercapacitor behavior is cycle dependent, data from cycles 3–10 were averaged and reported (unless otherwise noted).

Table 3 contains the average float current and decay time for the randomly oriented CNT electrodes (ROE_1 and ROE_2). The leakage or float current is similar for all supercapacitors examined in this preliminary study, an indication that the value may be dependent on the device architecture or the testing setup. In the case of the latter, the internal circuitry of the Arbin Supercapacitor Testing System or the control law(s) used to regulate the DUT voltage may generate measurement artifacts. As this DRI is a multi-year project, this potential measurement issue will be investigated in year 2 of the DRI. As indicated in table 3, lower charging currents (0.5 mA) had a tendency to have slightly prolonged decay times (1.5–3 times longer).

Table 3. Supercapacitor self-discharge data.

I_c (mA)	T_h (min)	Sample ID	I_{float} (mA)	T_{decay} (min)	V_d (mV)	Sample ID	I_{float} (mA)	T_{decay} (min)	V_d (mV)
0.5	0	ROE_1/G_1[a]	X	3.6 ± 0.7	50	ROE_2/G_1	X	67 ± 1	50
1	0	ROE_1/G_1[a]	X	1.3 ± 0.0	50	ROE_2/G_1	X	60 ± 2	50
2	0	ROE_1/G_1	X	X	X	ROE_2/G_1	X	56.9 ± 0.5	50
1	30	ROE_1/G_1	0.5 ± 0.3	88 ± 2	50	ROE_2/G_1	0.8 ± 0.2	42 ± 2	50
1	60	ROE_1/G_1	0.5 ± 0.3	52 ± 26	50	ROE_2/G_1	0.7 ± 0.2	120 ± 0	80
0.5	0	ROE_1/G_2	X	0.9 ± 0.0	50	ROE_2/G_2	X	41 ± 4	50
1	0	ROE_1/G_2	X	0.6 ± 0.0	50	ROE_2/G_2	X	31 ± 1	50
2	0	ROE_1/G_2	X	0.4 ± 0.0	50	ROE_2/G_2	X	49.6 ± 0.3	50
1	30	ROE_1/G_2	0.5 ± 0.3	120 ± 0	85	ROE_2/G_2	0.8 ± 0.1	63 ± 12	50
1	60	ROE_1/G_2	0.5 ± 0.4	62 ± 6	50	ROE_2/G_2	0.8 ± 0.1	99 ± 8	50
0.5	0	ROE_1/G_3	X	2.3 ± 0.1	50	ROE_2/G_3	X	43 ± 3	50
1	0	ROE_1/G_3[a]	X	1.3 ± 0.1	50	ROE_2/G_3[*]	X	24 ± 7	50
2	0	ROE_1/G_3	X	1.6 ± 0.0	50	ROE_2/G_3	X	10.0 ± 0.4	50
1	30	ROE_1/G_3	0.6 ± 0.3	120 ± 0	56	ROE_2/G_3	0.7 ± 0.2	120 ± 0	60
1	60	ROE_1/G_3	0.7 ± 0.2	18 ± 3	50	ROE_2/G_3	0.8 ± 0.1	71 ± 10	50
0.5	0	ROE_1/G_5	X	2.9 ± 0.0	50	ROE_2/G_5	X	38 ± 4	50
1	0	ROE_1/G_5	X	1.0 ± 0.2	50	ROE_2/G_5	X	26 ± 2	50
2	0	ROE_1/G_5	X	1.4 ± 0.0	50	ROE_2/G_5	X	26 ± 1	50
1	30	ROE_1/G_5	0.6 ± 0.3	120 ± 0	93	ROE_2/G_5	0.7 ± 0.2	91 ± 16	50
1	60	ROE_1/G_5	0.5 ± 0.3	45 ± 4	50	ROE_2/G_5	0.7 ± 0.2	86 ± 26	50

[a]Did not reach 1 V during all cycles. Only those cycles that did reach 1 V were averaged.

Note: I_c - charge current, T_h - hold time, I_{float} - float current, T_{decay} - average decay time, V_d - decay voltage, *X* - not available.

As the I_{float} values did not indicate which electrode composition and/or separator material had the best charge retention behavior, the self-discharge profiles of the supercapacitors were also recorded (table 3). For I_c = 1 mA and T_h = 0 min, supercapacitors constructed from ROE_2 had significantly longer decay times (24 min < T_{decay} < 60 min) than those constructed from ROE_1 (0.6 min < T_{decay} < 1.3 min), further supporting the results from galvanostatic charge-discharge tests. With the exception of supercapacitor ROE_2/G_1, which had a decay time of 60 min, randomly oriented CNT-based supercapacitors exhibited a weak charge retention behavior when the devices were not held in a charged state for an extended period of time. For ROE_1-based supercapacitors, the decay time was longest for hold times of 30 min. For ROE_2-based supercapacitors, T_{decay} varied depending on the separator material, with supercapacitors ROE_2/G_1 and ROE_2/G_2 having longer decay times for a hold time of 60 min and ROE_2/G_3 and ROE_2/G_5 having a longer decay time for a hold time of 30 min. As an example of this phenomenon, figure 13 contains the self-discharge behavior of supercapacitor ROE_1/G_2 and supercapacitor ROE_2/G_2 at various hold times. Although the mechanism for performance degradation for some supercapacitors at prolonged hold times (60 min) is not yet known, it may be the result of electrolyte degradation due to overcharging, corrosion of the current collector, or variations in the temperature of the testing environment (18.4 °C < RT < 28.2 °C). In an effort to mitigate temperature fluctuations in the testing environment, a dedicated air conditioning unit was installed in the laboratory. As can be seen in table 3, the overall decay time appears to be dependent on the charge current, hold time, and device properties. Of those supercapacitors

tested in this preliminary study, ROE_2/G_1 exhibited the best charge retention behavior, further supporting the results from galvanostatic charge-discharge tests. Nevertheless, the charge retention time of even ROE_2/G_1 is several orders of magnitude lower than commercial supercapacitors (e.g., reference 47). As this is a multi-year project, mechanisms for improving the leakage current of the CNT-based supercapacitors will be explored in year 2 of the project.

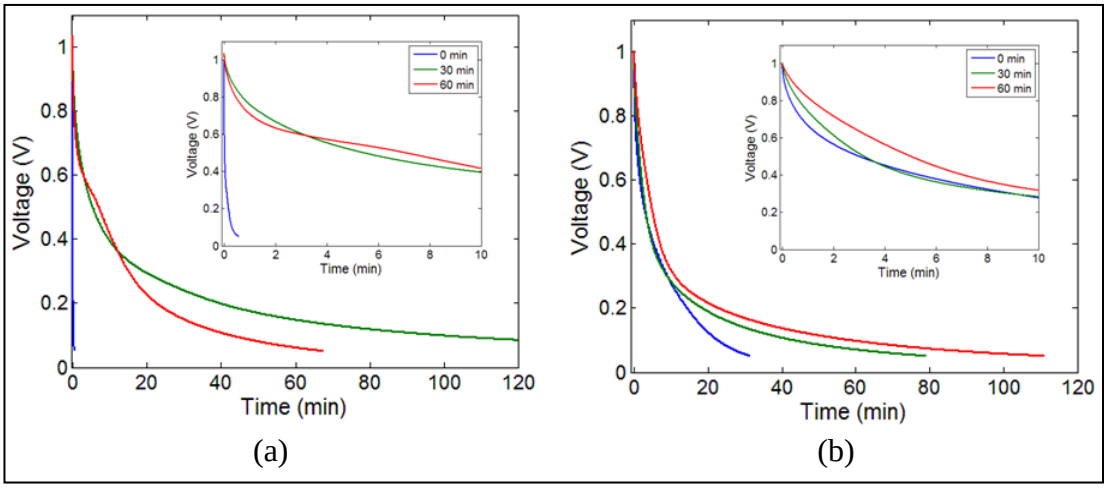

Figure 13. Self-discharge profile (I_c = 1 mA, cycle 10). Lines colors refer to the amount of time that the supercapacitor was held at the charged potential (1 V): Blue is 0 min, green is 30 min, and red is 60 min. (a) ROE_1/G_2 supercapacitor. (b) ROE_2/G_2 supercapacitor. Insets: Truncated time frames.

3.2.3 Cyclic Voltammetry

Electrochemical measurements were carried out on the randomly oriented and vertically aligned CNT-based supercapacitors at room temperature. Cyclic voltammograms for ROE_1- and ROE_2-based supercapacitors can be found in figure 14. Due to system noise (which was later resolved, see figure 15b), each of the curves shown in figure 14 was constructed from the average of 20–25 individual cyclic voltammograms. As the figure illustrates, the cyclic voltammograms have a rectangular core and do not contain the distinctive current peaks that are associated with redox reactions. The current increase around the voltage minima and maxima is believed to be due to electrolyte degradation or heterogeneous pore distribution in the separator material, with the grade 1 separator being the most heterogeneous of the four materials tested.

The cyclic voltammograms of the randomly oriented (ROE_1 and ROE_2) and vertically aligned (VAE_1) CNT-based supercapacitors can be found in figure 15. Of the three electrode materials tested, ROE_2 exhibited the best electrochemical performance, as indicated by the area enclosed by the cyclic voltammograms. The capacity and energy density of the vertically aligned CNT supercapacitor is negatively impacted by the interaction of the gel electrolyte ($LiPF_6$ in EC:DMC) with the polymers contained in the electrode. As indicated by the slope and enclosed area of the cyclic voltammogram shown in figure 15b, the polymer matrix we initially chose to investigate is believed to limit the ionic mobility of the organic electrolyte contained within the

device. As a result, we are currently exploring different polymer matrices and device architectures to improve the electrical behavior of the vertically aligned CNT-based supercapacitors.

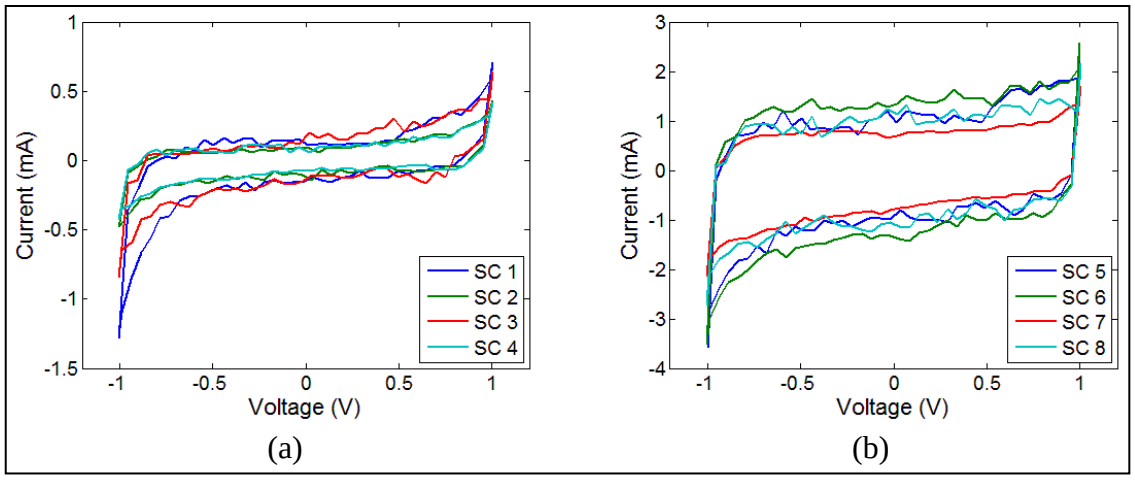

Figure 14. Average cyclic voltammograms of randomly oriented CNT-based supercapacitors. The CV measurements were carried out at a scan rate of 50 mV/s at room temperature. Blue is G_1, green is G_2, red is G_3, and cyan is G_5. (a) ROE_1 supercapacitor, (b) ROE_2 supercapacitor.

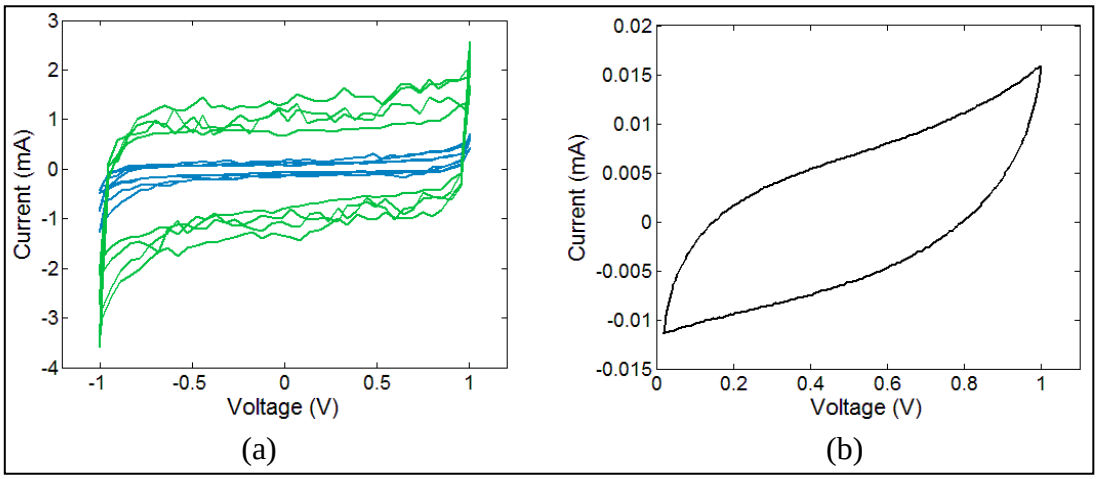

Figure 15. (a) Average cyclic voltammograms of randomly oriented CNT-based supercapacitors with 6M KOH electrolyte. The CV measurements were carried out at a scan rate of 50 mV/s at room temperature. Blue is ROE_1 and green is ROE_2. (b) Cyclic voltammogram of a polymer infiltrated vertically aligned CNT-based supercapacitor (VAE_1) with organic electrolyte ($LiPF_6$ in EC:DMC). The CV measurement was carried out at a scan rate of 0.5 mV/s at room temperature.

4. Conclusions

A major challenge in unmanned MV development stems from the lack of suitable energy storage devices. Demanding voltage and power requirements and stringent size and weight constraints significantly limit the number and type of batteries that can be housed in the MV structures. As a result, vehicle payloads and endurance times are significantly compromised. While the conventional approach is to create batteries with higher energy densities, an alternative approach is to replace structural components with multifunctional structural-energy storage materials. This current research effort has leveraged recent work in the areas of (1) lightweight, flexible, energy storage materials and (2) large-scale and high-stiffness multifunctional structural batteries, capacitors, and supercapacitors to develop lightweight, flexible, multifunctional structural-energy storage devices for MV applications.

The first year of this DRI effort explored several combinations of lightweight nanocomposites for multifunctional structural-energy storage applications. The energy storage devices studied initially were based on (1) randomly oriented CNT/polymer electrodes, (2) randomly oriented CNT/paper electrodes, and (3) vertically aligned CNT/polymer electrodes.

The baseline mechanical behavior of the CNT-ink-coated paper electrodes and the aligned CNT composite electrodes was established through uniaxial tensile tests. The elastic modulus and tensile strength of the CNT-ink-coated electrodes was found to be highly dependent on the loading direction and loading rates. The mechanical properties of the CNT-coated electrodes were also found to decrease by up to 25% after the multiple ink depositions that were required to fully coat the substrates. Commercial paper substrates coated with randomly oriented CNTs displayed mechanical behavior highly dependent on the loading direction and strain rate. Electrodes designed with vertically aligned CNTs displayed inherent flexibility as well as an elastic modulus approximately 250% higher than the neat PDMS/PVDF matrix.

The electrical behavior of supercapacitors fabricated with CNT-based electrodes was established through galvanostatic charge-discharge, self-discharge and CV tests. During year 1 of the project, three different electrode compositions (ROE_1, ROE_2, and VAE_1) and four different separator porosities (G_1, G_2, G_3, and G_5) were studied. ROE_2-based supercapacitors exhibited higher specific capacitance and better charge retention behavior than supercapacitors constructed from ROE_1 and VAE_1 electrodes. While preliminary, the results presented herein also indicate that an engineered separator material with a porosity and thickness similar to the G_1 separator may be most effective for aqueous (KOH) electrolytes. The cyclic voltammograms indicate that the capacity and energy density of VAE_1 supercapacitor was negatively impacted by polymer matrix material. Research focused on improving the specific capacitance of these randomly oriented and vertically aligned CNT devices will be continued in year 2 of the project.

5. References

1. Rivera, M. Current and Next-generation Energy Storage Devices for Micro Vehicle Applications. In *Proceedings of the SAE 2011 AeroTech Congress and Exhibition*, Toulouse, France, 2011.

2. Birkmeyer, P.; Peterson, K.; Fearing, R. DASH: A Dynamic 16g Hexapedal Robot. In *Proceedings of the 2009 IEEE/RSJ International Conference on Intelligent Robots and Systems*, St. Louis, MO, 2009.

3. Flynn, A.; Cylinder, D.; Dickinson, M.; Dickson, W.; Peek, M.; Hall, K.; Lebental, S.; Morris, S.; Tate, V.; Sandberg, W.; Ramamurti, R.; Geder, J.; Stux, A.; Swider-Lyons, K.; Stoman, R.; Crary, S.; Carter, S.; Carter, R.; Von Behrens, P.; Playter, R.; Cornelius, N.; Swilling, B.; Talebi, B.; Talebi, S.; deLasa, M.; Last, M.; Lanzisera, S.; Mehta, A. *Flapping Nano Air Vehicles*; MicroPropulsion Technical Report #100, 2010.

4. Luo, X.; Chung, D. Carbon-fiber/Polymer-matrix Composites as Capacitors. *Composites Science and Technology* **2001**, *61* (6), 885–888.

5. Thomas, J. P.; Qodwao, M. A. The Design and Application of Multifunctional Structure-battery Materials Systems. *JOM* **2005**, *57* (3), 18–24.

6. Pereira, T.; Guo, Z. H.; Nieh, S.; Arias, J.; Hahn, H. T. Embedding Thin-film Lithium Energy Cells in Structural Composites. *Composites Science and Technology* **2008**, *68* (7–8), 1935–1941.

7. Lin, Y. R.; Sodano, H. A. Characterization of Multifunctional Structural Capacitors for Embedded Energy Storage. *Journal of Applied Physics* **2009**, *106* (11), 114108.

8. Carlson, T.; Ordeus, D.; Wysocki, M.; Asp, L. E. Structural Capacitor Materials Made From Carbon Fibre Epoxy Composites. *Composites Science and Technology* **2010**, *70* (7), 1135–1140.

9. Gallagher, T.; Ciocanel, C.; Browder, C. Structural Load Bearing Supercapacitors Using a PEGDGE Based Solid Polymer Electrolyte Matrix. In *Proceedings of the ASME 2011 Conference on Smart Materials, Adaptive Structures and Intelligent Systems*, Phoenix, AZ, 2011.

10. O'Brien, D.; Baechle, D.; Wetzel, E. Multifunctional Structural Composite Capacitors for U.S. Army Applications. In *Proceedings of SAMPE 2006 Fall Technical Conference*, Dallas, TX, 2006.

11. Snyder, J. F.; Carter, R. H.; Wetzel, E. D. Electrochemical and Mechanical Behavior in Mechanically Robust Solid Polymer Electrolytes for use in Multifunctional Structural Batteries. *Chemistry of Materials* **2007**, *19* (15), 3793–3801.

12. Baechle, D.; O'Brien, D.; Wetzel, E. Design and Processing of Structural Composite Capacitors. In *Proceedings of SAMPE 2007*, Baltimore, MD, 2007.

13. Baechle, D.; O'Brien, D.; Wetzel, E. Structural Dielectrics for Multifunctional Capacitors. In *Proceedings of SPIE*, San Diego, CA, 2008.

14. Snyder, J.; O'Brien, D.; Baechle, D.; Mattson, D.; Wetzel, E. Structural Composite Capacitors, Supercapacitors, and Batteries for U.S. Army Applications. In *ASME Conference on Smart Materials, Adaptive Structures and Intelligent Systems*, Ellicott City, MD, 2008.

15. Snyder, J.; Wetzel, E.; Watson, C. Improving Multifunctional Behavior in Structural Electrolytes through Copolymerization of Structure- and Conductivity-promoting Monomers. *Polymer* **2009**, *50* (20), 4906–4916.

16. Snyder, J.; Wong, E.; Hubbard, C. Evaluation of Commercially Available Carbon Fibers, Fabrics, and Papers for Potential Use in Multifunctional Energy Storage Applications. *Journal of the Electrochemical Society* **2009**, *156* (3), A215–A224.

17. O'Brien, D.; Baechle, D. M.; Wetzel, E. D. Performance Metrics for Structural Composite Capacitors. In *Proceedings of the ASME 2010 Conference on Smart Materials, Adaptive Structures and Intelligent Systems*, Philadelphia, PA, 2010.

18. Ngo, E.; Snyder, J.; Hubbard, C.; Hirsch, S.; Xu, C.; Carter, R. *Development of Thin Films as Potential Structural Cathodes to Enable Multifunctional Energy-storage Structural Composite Batteries for the U.S. Army's Future Force*; ARL-TR-5644; U.S. Army Research Laboratory: Aberdeen Proving Ground, MD, September 2011.

19. Snyder, J.; Baechle, D.; Wetzel, E.; Xu, K. Multifunctional Structural Composite Batteries for U.S. Army Applications. In *Proceedings of the 26th Army Science Conference*, Orlando, FL, 2008.

20. Ervin, M. H.; Miller B. *Air Brush Fabricated Carbon Nanotube Supercapacitor Electrodes*; ARL-TR-5368; U.S. Army Research Laboratory: Adelphi, MD, September 2010.

21. Ervin, M.; Miller, B.; Hanrahan, B. *SWCNT Supercapacitor Electrode Fabrication Methods*; ARL-TR-5438; U.S. Army Research Laboratory: Adelphi, MD, February 2011.

22. Anton, C.; Ervin, M. *Carbon Nanotube Based Flexible Supercapacitors*; ARL-TR-5522; U.S. Army Research Laboratory: Adelphi, MD, April 2011.

23. An, K. H.; Jeon, K. K.; Heo, J. K.; Lim, S. C.; Bae, D.; Lee Y. High-capacitance Supercapacitor Using a Nanocomposite Electrode of Single-walled Carbon Nanotube and Polypyrrole. *Journal of the Electrochemical Society* **2002**, *149* (8), A1058–A1062.

24. Pushparaj, V. L.; Shaijumon, M. M.; Kumar, A.; Murugesan, S.; Ci, L.; Vajtai, R.; Linhardt, R. J.; Nalamasu, O.; Ajayan, P. Flexible Energy Storage Devices Based on Nanocomposite Paper. *Proceedings of the National Academy of Sciences of the United States of America* **2007**, *104* (34), 13574–13577.

25. Bruce, P. G.; Scrosati, B.; Tarascon J. M. Nanomaterials for Rechargeable Lithium Batteries. *Angewandte Chemie-International Edition* **2008**, *47* (16), 2930–2946.

26. Obreja, V.V.N. On the Performance of Supercapacitors with Electrodes Based on Carbon Nanotubes and Carbon Activated Material – A Review. *Physica E-Low-Dimensional Systems and Nanostructures* **2008**, *40* (7), 2596–2605.

27. Stoller, M. D.; Park, S. J.; Zhu, Y. W.; An, J. H.; Ruoff, R. S. Graphene-based Ultracapacitors. *Nano Letters* **2008**, *8* (10), 3498–3502.

28. Guo, Q. H.; Zhou, X. P.; Li, X. Y.; Chen, S. L.; Seema, A.; Greiner, A.; Hou, H. Q. Supercapacitors Based on Hybrid Carbon Nanofibers Containing Multiwalled Carbon Nanotubes. *Journal of Materials Chemistry* **2009**, *19* (18), 2810–2816.

29. Hu, L. B.; Choi, J. W.; Yang, Y.; Jeong, S.; La Mantia, F.; Cui, L. F.; Cui, Y. Highly Conductive Paper for Energy-storage Devices. *Proceedings of the National Academy of Sciences of the United States of America* **2009**, *106* (51), 21490–21494.

30. Meng, C. Z.; Liu, C. H.; Chen, L. Z.; Hu, C. H.; Fan, S. S. Highly Flexible and All-solid-state Paperlike Polymer Supercapacitors. *Nano Letters* **2010**, *10* (10), 4025–4031.

31. Nayfeh, O.; Chin, M.; Ervin, M.; Wilson, J.; Ivanov, T.; Proie, R.; Nichols, B.; Crowne, F.; Kilpatrick, S.; Dubey, M.; Nambaru, R.; Ulrich, M. *Graphene-based Nanoelectronics*; ARL-TR-5451; U.S. Army Research Laboratory: Adelphi, MD, February 2011.

32. Hu, L. B.; Yuan, W.; Brochu, P.; Gruner, G.; Pei, Q. Highly Stretchable, Conductive, and Transparent Nanotube Thin Films. *Applied Physics Letters* **2009**, *94* (16), 161108.

33. Schrage, C.; Kaskel, S. Flexible and Transparent SWCNT Electrodes for Alternating Current Electroluminescence Devices. *ACS Applied Materials and Interfaces* **2009**, *1* (8), 1640–1644.

34. Hu, L.; Pasta, M.; La Mantia, F.; Cui, L.; Jeong, S.; Deshazer, H.; Choi, J.; Han, S.; Cui Y. Stretchable, Porous, and Conductive Energy Textiles. *Nano Letters* **2010**, *10* (2), 708–714.

35. Park, M.; Kim, H.; Youngblood, J. P. Strain-dependent Electrical Resistance of Multi-walled Carbon Nanotube/Polymer Composite Films. *Nanotechnology* **2008**, *19* (5), 055705.

36. Oliva-Aviles, A. I.; Aviles, F.; Sosa, V. Electrical and Piezoresistive Properties of Multi-walled Carbon Nanotube/Polymer Composite Films Aligned by an Electric Field. *Carbon*, **2011**, *49* (9), 2989–2997.

37. Yamada, T.; Hayamizu, Y.; Yamamoto, Y.; Yomogida, Y.; Izadi-Najafabadi, A.; Futaba, D. N.; Hata, K. A Stretchable Carbon Nanotube Strain Sensor for Human-motion Detection. *Nature Nanotechnology* **2011**, *6* (5), 296–301.

38. Xie, X.; Bai, H.; Shi, G.; Qu, L. Load-tolerant, Highly Strain-responsive Graphene Sheets. *Journal of Materials Chemistry* **2011**, *21* (7), 2057–2059.

39. Eswaraiah, V.; Balasubramaniam, K.; Ramaprabhu, S. Functionalized Graphene Reinforced Thermoplastic Nanocomposites as Strain Sensors in Structural Health Monitoring. *Journal of Materials Chemistry* **2011**, *21* (34), 12626–12628.

40. Goyal, A.; Reddy, A.; Ajayan, P. Flexible Carbon Nanotube-Cu_2O Hybrid Electrodes for Li-ion Batteries. *Small* **2011**, *7* (12), 1709–1713.

41. Small, W.; Masdarolomoor, F.; Wallace, G.; Panhuis, M. Inkjet Deposition and Characterization of Transparent Conducting Polyaniline Composite Films with a High Carbon Nanotube Loading Fraction. *Journal of Materials Chemistry* **2007**, *17* (41), 4359–4361.

42. Hahm, M.; Kwon, Y.; Lee, E.; Ahn, C.; Jung, Y. Diameter Selective Growth of Vertically Aligned Single Walled Carbon Nanotubes and Study on Their Growth Mechanism. *The Journal of Physical Chemistry C* **2008**, *112*, 17143–17147.

43. Stux, A.; Swider-Lyons, K. *Survey of Commercial Small Lithium Polymer Batteries*; NRL/MR/6110--07-9073; U.S. Naval Research Laboratory: Washington, DC, September 19, 2007.

44. Haslach, H.; Armstrong, R. *Deformable Bodies and Their Material Behavior*, Hoboken, NJ: John Wiley & Sons, Inc., 2004.

45. Bradford, P.; Wang, X.; Zhao, H.; Maria, J.; Jia, Q.; Zhu, Y. A Novel Approach to Fabricate High Volume Fraction Nanocomposites with Long Aligned Carbon Nanotubes. *Composites Science and Technology* **2010**, *70*, 1980–1985.

46. Ogasawara, T.; Moon, S.; Inoue, Y.; Shimamura, Y. Mechanical Properties of Aligned Multi-walled Carbon Nanotube/Epoxy Composites Processed Using a Hot-melt Prepreg Method. *Composites Science and Technology* **2011**, *71*, 1826–1833.

47. Maxwell Technologies, Inc. *Maxwell Technologies Product Comparison Matrix* 30 09 2011. www.maxwell.com (accessed 29 November 2011).

48. Whatman, “Whatman.” http://www.whatman.com/QualitativeFilterPaperStandardGrades.aspx (accessed May 2011).

6. Transitions

6.1 Transitions into Developmental Army Programs

This research effort is primarily concerned with the development of lightweight structural/energy storage composites for MV applications. Within ARL, the Micro Autonomous Systems and Technology (MAST) program has identified energy storage as a key issue for the development of MVs. The broader impact of this work is the development of lightweight multifunctional building blocks for portable electronic systems, which could be of interest to such Army organizations as the Aviation and Missile Research, Development and Engineering Center (AMRDEC) and Communications-Electronics Research Development and Engineering Center (CERDEC).

6.2 Documentation

- Cole, D. P.; Rivera M.; Bundy M. Characterization of Mechanical Properties in Multifunctional Structural-energy Storage Nanocomposites for Lightweight Micro Autonomous Systems, In *Proceedings of the ASME 2011 Conference on Smart Materials, Adaptive Structures and Intelligent Systems*, Phoenix, AZ, 2011.
- Rivera M.; Cole, D. P; Bundy M. Electrical Properties of Carbon Nanomaterial-based Structural-energy Storage Devices, In *Proceedings of the ASME 2011 Conference on Smart Materials, Adaptive Structures and Intelligent Systems*, Phoenix, AZ, 2011.
- Rivera, M. Current and Next-Generation Energy Storage Devices for Micro Vehicle Applications, In *Proceedings of the SAE 2011 AeroTech Congress and Exhibition*, Toulouse, France, 2011.

6.3 Presentations

- Rivera, M.; Cole, D. P; Bundy, M. Electrical Properties of Carbon Nanomaterial-based Structural-energy Storage Devices," *ASME 2011 Conference on Smart Materials, Adaptive Structures and Intelligent Systems*, Phoenix, AZ, September 20, 2011.
- Cole, D. P; Rivera M.; Bundy, M. Characterization of Mechanical Properties in Multifunctional Structural-energy Storage Nanocomposites for Lightweight Micro Autonomous Systems," *ASME 2011 Conference on Smart Materials, Adaptive Structures and Intelligent Systems*, Phoenix, AZ, September 20, 2011.
- Rivera, M. Current and Next-Generation Energy Storage Devices for Micro Vehicle Applications," *SAE 2011 AeroTech Congress and Exhibition*, Toulouse, France, October 20, 2011.

List of Symbols, Abbreviations and Acronyms

AMRDEC	Aviation and Missile Research, Development and Engineering Center
ARL	U.S. Army Research Laboratory
ASME	American Society of Mechanical Engineers
CERDEC	Communications-Electronics Research Development and Engineering Center
CD	cross-machine direction
CNT	carbon nanotube
COTS	commercial-off-the-shelf
C_{sp}	specific capacitance
CV	cyclic voltammetry
CVD	chemical vapor deposition
DARPA	Defense Advanced Research Projects Agency
DASH	Dynamic Autonomous Sprawled Hexapod
DI-H_20	deionized water
DMC	dimethyl carbonate
DMF	dimethylformamide
DRI	Director's Research Initiative
DUT	device under test
EC	ethylene carbonate
EDLC	electric double layer capacitor
G_{1-5}	cellulose filter paper grades
I_c	charge current
I_d	discharge current
I_{float}	float current
KOH	potassium hydroxide

$LiPF_6$	lithium hexafluorophosphate
MAST	micro autonomous systems and technology
MAV	micro aerial vehicle
MD	machine direction
MV	micro vehicle
MWNT	multi-walled nanotube
PDMS	polydimethylsiloxane
PVDF	polyvinylidene fluoride
ROE	randomly oriented CNT-based electrode
RT	room temperature
SC	supercapacitor
SDBS	sodium dodecylbenzenesulfonic acid
SEM	scanning electron microscope
TAPPI	Technical Association of the Pulp and Paper Industry
T_{charge}	charge time
T_{decay}	decay time
$T_{discharge}$	discharge time
TEM	transmission electron microscope
T_h	hold time
VAE	vertically aligned CNT-based electrode
V_d	decay voltage

No of. Copies	Organization
1 ELEC	ADMNSTR DEFNS TECHL INFO CTR ATTN DTIC OCA 8725 JOHN J KINGMAN RD STE 0944 FORT BELVOIR VA 22060-6218
10 HCS	US ARMY RESEARCH LAB ATTN RDRL VTM DANIEL P COLE (2 CPS) MONICA RIVERA (2 CPS) MARK BUNDY (3 CPS) DY LE MARK VALCO ATTN RDRL WM SHASHI KARNA ABERDEEN PROVING GROUND MD 21005
9 HCS	US ARMY RSRCH LAB ATTN IMNE ALC HRR MAIL & RECORDS MGMT ATTN RDRL CIO LL TECHL LIB ATTN RDRL CIO LT TECHL PUB ATTN RDRL SER L M ERVIN ATTN RDRL SER L M DUBEY ATTN RDRL SER L B PIEKARSKI ATTN RDRL-SED-C C. LUNDGREN ATTN RDRL SED C C XU ATTN RDRL SER P AMIRTHARAJ ADELPHI MD 20783-1197
4 HCS	US ARMY RSRCH LAB ATTN RDRL WMM E E NGO ATTN RDRL-WMM-A E WETZEL ATTN RDRL-WMM-A D. OBRIEN ATTN RDRL WMM G J SNYDER BLDG 4600 ABERDEEN PROVING GROUND MD 21005

TOTAL: 24 (23 HCS, 1 PDF)